Study of Sentinel-3/SLSTR suitability for estimating active fire parametres

Abel Calle

University of Valladolid, Dpt. of Applied Physics, Valladolid, Spain; abel.calle@fa1.uva.es

Abstract. FRP (Fire Radiative Power) is the magnitude associated to the thermal radiance which explains the ecological effects of active fire; it is the component of the chemical power released from burning vegetation and emitted as radiation during the process of combustion. In this paper, a discussion of the procedures for active fire FRP is presented: The Dozier method, originally developed for use with the AVHRR (Advanced Very High Resolution Radiometer), the MODIS (Moderate Resolution Imaging Spectroradiometer) fire detection algorithm and semi-empirical relationship based on previous studies of BIRD (Bi-spectral InfraRed Detection) satellite. These procedures, described above, are applied to simulated data by a radiative transfer model, based on Sentinel-3/SLSTR spectral characteristics in order to analyze the impact of atmospheric conditions on FRP estimations.

Keywords. Sentinel-3, SLSTR, Forest fires, Fire Radiative Power.

1. Introduction

FRP (Fire Radiative Power) is the magnitude associated to the thermal radiance which explains the ecological effects of active fire; it is the component of the chemical power released from burning vegetation and emitted as radiation during the process of combustion. FRP was introduced by [1] as a useful magnitude to estimate biomass combustion rates and the associated emissions.

The Dozier method, originally developed for use with the AVHRR (Advanced Very High Resolution Radiometer) is a bi-spectral technique using radiance in the MIR (Middle InfraRed, 3–4 μm) and TIR (Thermal InfraRed, 10–12μm) to estimate the pixel fraction affected by fire and the fire temperature [2], both involved in the FRP estimation. Nevertheless, the monitoring of fire using remote sensing presents sources of uncertainty due to unexpected atmospheric conditions and unknown values of emissivity, among other aspects, so the Dozier's bi-spectral equations must be solved using numeric methods. Concerning polar orbiting satellites, the MODIS (Moderate Resolution Imaging Spectroradiometer) fire detection algorithm [3] is a reference methodology which can be applied to other sensors. The MODIS fire product, described in [4], proposes FRP estimation using an empirical relationship with brightness temperature, thus avoiding having to solve the bi-spectral equations. Using the MODIS algorithm as the baseline, [5] have developed an active fire detection algorithm, to be implemented on Sentinel-3/SLSTR (Sea and Land Surface Temperature Radiometer) sensor, with successfully validated results. In order to estimate the FRP, they propose using a semi-empirical relationship based on previous studies of BIRD (Bi-spectral InfraRed Detection) satellites [6].

The GMES (Global Monitoring for Environment and Security), is an initiative of the European Commission and the ESA which objective is evaluate the European capacity for the provision and use of operational services. The contribution of GMES to the topic of forest fires is represented by the future satellite Sentinel-3: today, with the interruption of Envisat services, the study of suitability of algorithms to be implemented on Sentinel-3 is a necessary scientific task.The future instrument SLSTR, described in [7], is an improved continuation of Envisat/AATSR (Advanced Along-Track Scanning Radiometer) that will be put into operation within the European GMES (Global

Monitoring for Environment and Security) programme. SLSTR will provide measurements in nine spectral channels, two of which are optimised for fire monitoring. The Sentinel-3 mission's main objective is to measure sea-surface topography, sea- and land-surface temperature and ocean- and land-surface colour with high-end accuracy and reliability in support of ocean forecasting systems, and for environmental and climate monitoring. The SLSTR (Sea and Land Surface Temperature Radiometer) sensor improves the along-track-scanning dual-view technique of AATSR and provides advanced atmospheric correction. SLSTR measures in nine spectral channels, with two bands optimised for fire monitoring, covering the spectral region [0.55-12] μm. The SLSTR has a spatial resolution in the visible and shortwave infrared channels of 500 m and 1 km in the thermal infrared channels. Table 1(adapted from [7]) shows the thermal spectral bands (with a spatial resolution of 1 km), and its radiometric performances; note that spectral bands devoted to fire observation are F1 and F2.

Table 1. Radiometric performances for thermal spectral bands of the SLSTR sensor. This table is adapted from [7], where an extensive description of SLSTR sensor can be found.

Ch.	Band	λ (μm)	Δλ (μm)	T range (K)	T Ref. (K)	NEΔT Ref. (mK)
S7	MIR	3.74	0.38	200–323	270	56
S8	TIR	10.85	0.9	200–321	270	29
S9	TIR	12	1.0	200–318	270	21
F1	MIR	3.74	0.38	285–500	285–500	680–16
F2	TIR	10.85	0.9	230–400	230–400	79–35

λ is the central wavelength, Δλ is the spectral width, albedo is the top of atmosphere reflectance, T is the top of atmosphere brightness temperature, SNR is the signal-to-noise ratio, and NEΔT is the noise equivalent temperature difference.

In this letter, a discussion of the aforementioned procedures for active fire FRP is presented. These procedures, described above, are applied to simulated data by a radiative transfer model, based on SLSTR spectral characteristics in order to analyze the impact of atmospheric conditions on FRP estimations.

2. Technical approaches to FRP estimation

The fire parameters, fire temperature, Tf, and burning pixel fraction, p, can be obtained by means of Dozier's methodology [2], which is based on the solution of the following system of equations:

$$\begin{cases} L_{MIR} = p\,B(\lambda_{MIR}, T_f) + (1-p)\,B(\lambda_{MIR}, T_{suf}) \\ L_{TIR} = p\,B(\lambda_{TIR}, T_f) + (1-p)\,B(\lambda_{TIR}, T_{surf}) \end{cases} \qquad 0 < p < 1 \tag{1}$$

where L_{MIR} and L_{TIR} are the outgoing radiances from the pixel, at surface level, in the spectral regions of 3–4 μm and 11 μm, respectively, and B(λ,T) is the Planck function involving wavelength, λ, and temperature, T. T_{surf} is the temperature of the background not affected by the fire. A more realistic scheme, including reflective terms in the MIR spectrum and atmospheric transmittance, is described by [8]; this letter ignores reflective terms. The FRP is estimated by means of the Stefan-Boltzmann law:

$$FRP = pA_{sampl}\sigma T_f^4 \tag{2}$$

where A_{sampl} is the total pixel area (in km^2), σ is the Stefan–Boltzmann constant (5.67×10^{-8} $Wm^{-2}K^{-4}$) and FRP is in MW.

In the MODIS fire product [4], the FRP is estimated using the empirical relationship of [9]:

$$FRP_{8th} = C\left(T_{MIR}^8 - \overline{T}_{MIR}^8\right)A_{sampl} \quad (3)$$

where T_{MIR} is the 4 μm brightness temperature of the fire pixel detected, $\overline{T}_{MIR}$ is the average of 4 μm brightness temperature of the background (no fire), and A_{sampl} is the total area (in km^2) of the pixel. C is an empirical constant determined on the MODIS 4 μm spectral channel ($C_{MODIS}=4.34\times10^{-19}$ $MWK^{-8}km^{-2}$). The FRP (in MW) is hereafter called FRP_{8th}, due its dependence on the 8^{th} power of brightness temperature.

An algorithm for active fire detection has been proposed to be applied on the Sentinel-3 SLSTR sensor by [5]. For each pixel affected by fire, the FRP is calculated using the MIR radiance by means of the method explained in [6]:

$$FRP_{4th} = \frac{A_{sampl}}{10^6\,\tau_{MIR}}\left(\frac{\sigma}{a}\right)\left(L_{MIR} - \overline{L}_{MIR}\right) \quad (4)$$

where A_{sampl} is the ground projection area of the sensor FOV (Field Of View) in m^2, and which is zenith angle view dependent, σ is the Stefan–Boltzmann constant, L_{MIR} is the MIR channel spectral radiance of the fire pixel ($Wm^{-2}sr^{-1}\mu m^{-1}$), $\overline{L}_{MIR}$ is the mean MIR channel spectral radiance of the background pixels ($Wm^{-2}sr^{-1}\mu m^{-1}$), τ_{MIR} is the atmospheric transmissivity in the MIR spectral band (calculated as a function of the total column of water vapour content) and a ($Wm^{-2}sr^{-1}\mu m^{-1}K^{-4}$) is the factor of the relationship between the spectral radiance and the fourth power of the temperature; that is: the spectral radiance $L(\lambda,T)$ emitted by a black body at wavelength λ is given by the Planck function, which can be approximated over the MIR temperature range (around 4 μm) by the simple power law: $L(\lambda)=aT^{4.0}$; note the radiance method is only valid for fire temperatures above 600K; there is no linear behaviour below this value. FRP_{4th} is expressed in MW.

3. Methodology

A series of fires have been simulated by means of the MODTRAN (MODerate resolution atmospheric TRANsmission) [10] in order to calculate the outgoing radiance at TOA (Top of Atmosphere) and received by the SLSTR sensor. The scenarios of simulated data are described by the intervals of the parameters: $T_f \in [400K,1100K]$, $p \in [1e\text{-}5,0.4]$ and atmospheric transmittance $\tau_{MIR} \in [0.69,0.88]$; τ_{TIR} was calculated so that the τ_{MIR} and τ_{TIR} were linked to standard atmospheric profiles (random variations between them were not considered). The spectral radiance was integrated using square spectral response functions for SLSTR fire channels, F1 (λ= 3.74 μm, $\Delta\lambda$= 0.38μm) and F2 (λ= 10.85 μm, $\Delta\lambda$= 0.9 μm) (see [7] for a detailed description of the SLSTR instrument), using a nominal value of A_{sampl} of 1 km^2. The FRP of the simulated fires, hereafter called FRP_{TRUE}, was calculated by means of input simulation values of p and T_f and eq. (2) (Note that FRP_{TRUE} is not dependent on atmospheric transmission). The temperature of the surface not affected by fire (background) was considered as 300K. In order to consider representative emissivity values, for the background, ε_{MIR}=0.85 (channel of 3.74 μm) and ε_{TIR}=0.9 (channel of 10.85 μm) were used, and fire was considered as a black body. Although these values are very low for green vegetation, they are suitable for senescent vegetation, in accordance with [11] and [12].

To estimate FRP by means of the Dozier plus Stefan-Boltzmann (FRP_{DSB} hereafter), an iterative algorithm is proposed here; it is based on TOA MIR and TIR radiances received by the sensor, according to the following equations:

$$L_j = \tau_j pB(\lambda_j, T_f) + (1-p)\bar{L}_j \quad j = MIR, TIR \tag{5}$$

where j is the spectral channel (MIR and TIR), L_j is the TOA radiance provided by the sensor, τ_j is the atmospheric transmittance, $B(\lambda,T)$ is the Planck function, T_f is the fire temperature, p is the pixel fraction affected by fire, and $\bar{L}_j$ is the average of the TOA radiance of background pixels; note that this term includes the atmospheric transmittance and emissivity dependence. In order to find T_f, the equation (6) is solved by a iteration procedure:

$$\frac{\left(L_{MIR} - \bar{L}_{MIR}\right)}{\tau_{MIR} B(\lambda_{MIR}, T_f) - \bar{L}_{MIR}} = \frac{\left(L_{TIR} - \bar{L}_{TIR}\right)}{\tau_{TIR} B(\lambda_{TIR}, T_f) - \bar{L}_{TIR}} \tag{6}$$

The fire fraction, p, is estimated, finally, from any of the equations (5) and the FRP (FRP_{DSB} hereafter) is obtained from eq. (2). Taking into account the fact that atmospheric conditions are unknown when the method is applied, an average of τ_{MIR} and τ_{TIR}, used in the simulation of fires, were used. The error in T_f and p are negligible when atmospheric transmittance and the corresponding radiance are used in the simulation; when an averaged transmittance is used, the maximum errors found, in the described interval of transmittance, were 60K, in T_f, and 70%, in p (for $p=10^{-3}$). Note that the impact on the estimate of FRP, due to p error is much smaller than the T_f error.

Concerning the estimation of FRP_{8th}, used in the MODIS fire product, a new empirical constant for SLSTR was calculated, C_{SLSTR}, to be used in eq. (3). This only used the not saturated values, the fire temperature and the atmospheric transmittance described in the simulated fires; so, using FRP simulated values and spectral features of the SLSTR sensor, the constant $C_{SLSTR}=4.48\times10^{-19}$ $MWK^{-8}km^{-2}$ was estimated by means of a linear regression (determination coefficient, $R^2=0.94$). Note that C_{SLSTR} is slightly different from C_{MODIS}.

The methodology applied to FRP_{4th} described by eq. (4) is not suitable for fire temperatures below 600 K. The "a" constant valid for the SLSTR sensor, previously estimated by means of averaged atmospheric transmittances used on the simulated fires, was $a_{SLSTR}=1.05\times10^{-9}$ $Wm^{-2}sr^{-1}\mu m^{-1}K^{-4}$ ($R^2=0.99$).

4. Results and discussion

The error percentage provided by the FRP_{DSB} is not dependent on the fire fraction. The error increases with τ_{MIR} and τ_{TIR} and decreases with T_f. The restriction of this procedure is that, for T_f lower than 450K, there is no convergence in the eq. (6). These results are summarised in figure 1.

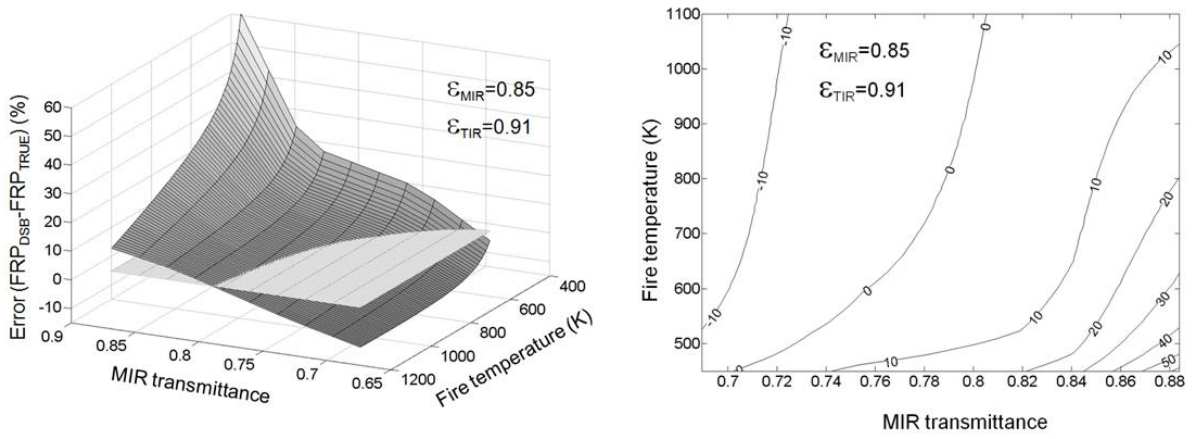

Figure 1. Percentage of error, in the FRPDSB estimation; Left: the error graph as function of MIR transmittance and fire temperature; the level of error 0% is shown as reference. Right: Error contours generated by 3D graph intersection with error planes [-10%, 50%].

The percentage of error provided by FRP_{8th} shows a strong dependence on the fire fraction when the fire temperature increases. Figure 2 shows the 3D graph of errors for three p values (10^{-1}, 10^{-2} and 10^{-3}). Note that $p=10^{-1}$ is incomplete due to the SLSTR sensor saturation (saturation occurs for T_f above 740 K for $p=10^{-1}$). The dependence on τ_{MIR} is weak. FRP_{8th} exhibits a good behaviour, with errors inside the interval ±10%, for $p=10^{-2}$, for $T_f \in [540K,600K]$ for high τ_{MIR} and $T_f \in [600K,740K]$ for lower τ_{MIR} values. If p decreases, the error range ±10% corresponds to T_f intervals narrower and shifted to a lower T_f. These results are summarised in figure 2.

The percentage of error provided by FRP_{4th} does not show any dependence on the fire fraction. Higher τ_{MIR} values are more sensitive to errors, so FRP_{4th} is inside the interval ±10% for the interval $T_f \in [625K,700K]$ for high τ_{MIR} and $T_f \in [720K,900K]$ for lower τ_{MIR} values. FRP_{4th} overestimates FRP_{TRUE} for high T_f. These results are summarised in figure 3.

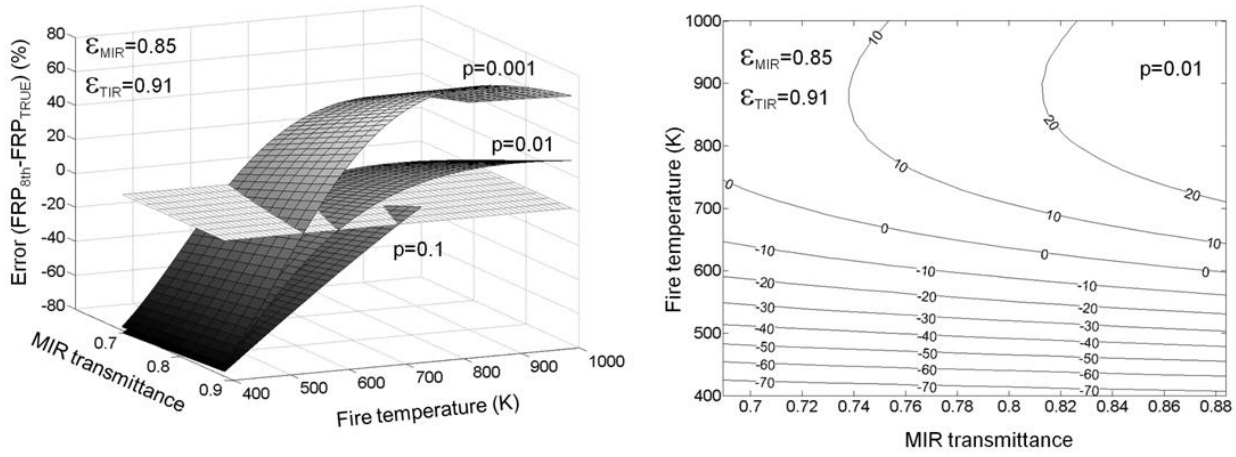

Figure 2. Percentage of error, in the FRP8th estimation. Left: Error graph as function of MIR transmittance, fire temperature and fire fraction; the level of error 0% is shown as reference. Note p=0.1 is incomplete due to SLSTR saturation. Right: Error contours generated by intersection of the 3D graph, in p=10-2, with planes of error [-70%, 20%].

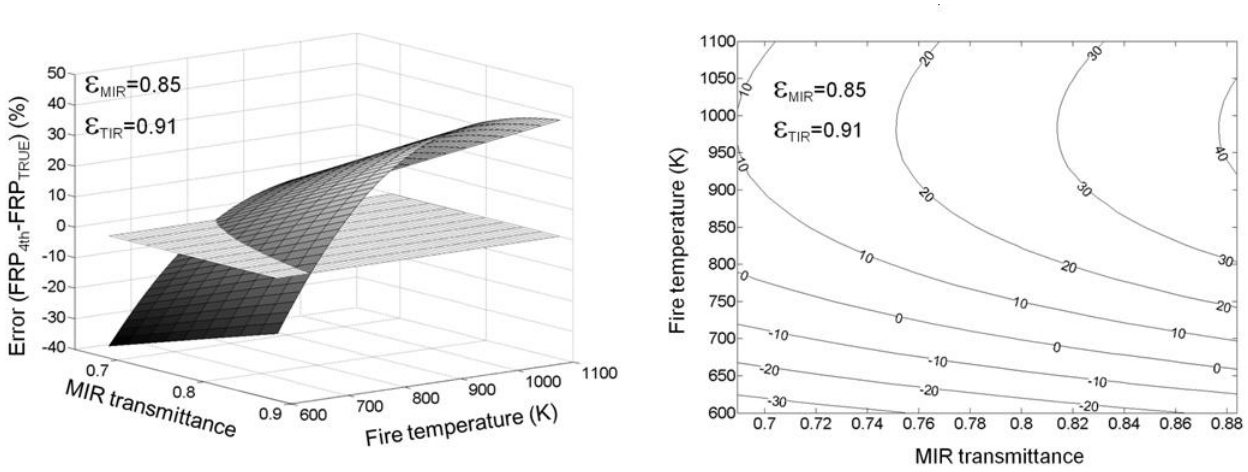

Figure 3. Percentage of error, in the FRP_{4th} estimation. Top: Error graph as function of MIR transmittance and fire temperature; the level of error 0% is shown as reference. Bottom: Error contours generated by the intersection of the 3D graph with planes of error [-30%, 40%].

This analysis has been performed taking into account a senescent vegetation scenario covering the background (regarding emissivity values). Nevertheless, the same analysis was performed previously considering a black body background; the same errors have been found for the three algorithms. Note the spectral radiance or brightness temperature used by them is a TOA magnitude. For the fire fraction, however, black body behaviour may reasonably be assumed, provided the line-of-sight path length through the flames is sufficiently thick [13]; so eq. (5) does not include the emissivity correction.

The shape of the spectral response function was also analysed in order to find out its impact on the final FRP estimations. A Gaussian shape was simulated, excelling the top-hat shape, left and right, in response 0.2. This spectral response function is slightly different to the previous shape due to the integrated radiance at left and right of the top-hat; for example, for the case p=0.001, differences in brightness temperature are 0.3K (MIR) and 3.2K (TIR). Nevertheless, the errors found in the fire temperature and fire fractions affected by the fire are the same as those mentioned previously (±2.6% on average). So, the FRP procedures described here will not be dependent on the final shape of the SLSTR spectral response function. Note the figure 4 when a comparison between square and gaussian Spectral Response Function is shown.

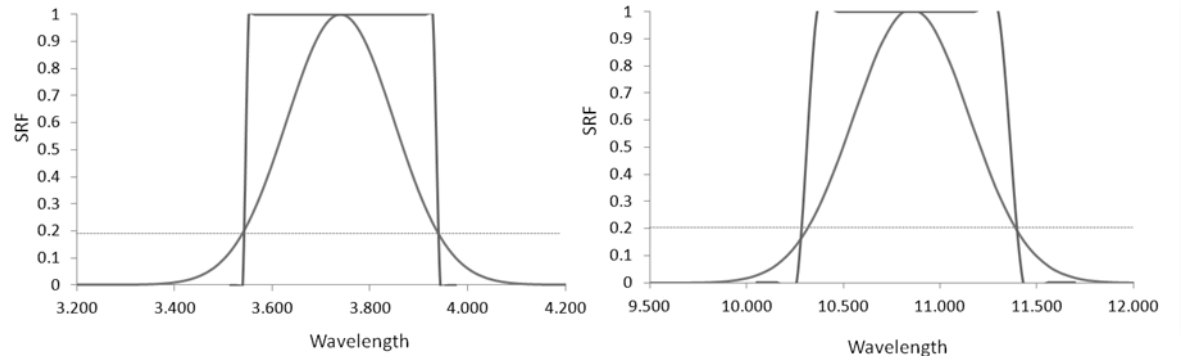

Figure 4: Two different SRF were considered for each spectral channel: gaussian and square SRF. The gaussian function was strongly forced to overpass the requirements of square function, in order to calculate the impact of this issue in the radiance obtained by the sensor.

Finally, the future SLSTR sensor will be suitable for fire monitoring because the saturation of the MIR channel only occurs in scenarios with a high fire power (Fire temperature, burning area); for example: from (980K, 2.5ha), (840K, 5ha), (770K, 7.5ha), (730K, 10ha), (670K, 15ha).

5. Conclusion

The methods FRP_{4th} and FRP_{DSB} show better results in larger interval of fire temperature than the FRP_{8th} procedure and, moreover, they show no dependence on the fire fraction. However, the errors caused by them increase dramatically when the fire temperature falls below a certain value: 450 K for FRP_{DSB} due to uncertainty in the convergence of equation (6) and 650 K for FRP_{4th} due to relationship radiance versus $T^{4.0}$ is not valid; this is a restriction of the method when the confidence level (in the fire detection) is low. Note that a small fire, or a fire with a low temperature, is difficult to detect.

The FRP_{DSB} method shows better results than the FRP_{4th} and FRP_{8th}, and its applicability range is larger; however, it is more sensitive to unknown atmospheric transmittance and uses τ_{MIR} and τ_{TIR}.

The lack of knowledge concerning atmospheric conditions seems to be the most important source of errors, in estimating the FRP. Therefore, other specific atmospheric factors should be taken into account, such as smoke and aerosols. Also, the SLSTR sensor presents good performances in avoiding saturation.

All the results and comparisons are derived by the analysis of Sentinel/SLSTR simulated data and, as a result, certain limitations exist with the use of these data, while expectations should rise from the use of the original data in the future.

References

[1] Kaufman, Y., Remer, L., Ottmar, R., Ward, D., Rong-R, L., Kleidman, R., Fraser, R., Flynn, L., McDougal, D. and Shelton, G. (1996). Relationship between remotely sensed fire intensity and rate of emission of smoke: SCAR-C experiment. *In J. Levine (Ed.), Global biomass burning*. (pp. 685– 696). MA: MIT Press.

[2] Dozier, J. (1981). A method for satellite identification of surface temperature fields of subpixel resolution. *Remote Sensing of Environment*, 11, 221-229.

[3] Giglio, L., Descloitres, J., Justice, C.O. and Kaufman, Y.J. (2003). An enhanced contextual fire detection algorithm for MODIS. *Remote Sensing of Environment*, 87:273-282.

[4] Justice, C., Giglio, L., Boschetti, L, Roy, D., Csiszar, I, Morisette, J. and Kaufman, Y. (2006). MODIS Fire Products. *Algorithm Technical Background Document, version 2.3, 1 October 2006*, EOS ID# 2741. MODIS Science Team, (p. 12)

[5] Wooster, M.J., Xu, W. and Nightingale, T. (2012). Sentinel-3 SLSTR active fire detection and FRP product: Pre-launch algorithm development and performance evaluation using MODIS and ASTER datasets. *Remote Sensing of Environment*, 120, 236-254.

[6] Wooster, M.J., Zhukov, B. and Oertel, D. (2003). Fire radiative energy for quantitative study of biomass burning: derivation from the BIRD experimental satellite and comparison to MODIS fire products. *Remote Sensing of Environment*, 86, 83-107.

[7] Coppo, P., Ricciarelli, B., Brandani, F., Delderfield, J., Ferlet, M., Mutlow, C., Munro, G., Nightingale, T., Smith, D., Bianchi, S., Nicol, P., Kirschstein, S., Hennig, T., Engel, W., Frerick, J. and Nieke, J. (2010). SLSTR: a high accuracy dual scan temperature radiometer for sea and land surface monitoring from space. *Journal of Modern Optics*, 57: 18, 1815-1830

[8] Giglio, L. and Kendall, J.D., (2001). Application of the Dozier retrieval to wildfire characterization. A sensitivity analysis. *Remote Sensing of Environment*, 77, 34-49.

[9] Kaufman, Y. J., Justice, C. O., Flynn, L. P., Kendall, J. D., Prins, E. M., Giglio, L., Ward, D. E., Menzel, W. P. and Setzer, A. W., (1998). Potential global fire monitoring from EOS-MODIS. *Journal of Geophysical Research*, 103:32215-32238.

[10] Berk, A., Bernstein, L.W. and Robertson, D.C. (1996). MODTRAN: A moderate resolution model for LOWTRAN 7, *Rep. AFGL-TR-83-0187, Philips Lab*., Hanscom Air Force Base, Mass.
[11] Salisbury, J., W. and D'Aria, D. (1994). Emissivity of Terrestrial Materials in the 3-5/ m Atmospheric Window. *Remote Sensing of Environment*, 47:345-361.
[12] Salisbury, J., W. and D'Aria, D. (1994). Emissivity of Terrestrial Materials in the 8-14/tm Atmospheric Window. *Remote Sensing of Environment*, 42:83-106.
[13] Langaas, S. (1995). A critical review of sub-resolution fire detection techniques and principles using thermal satellite data. *PhD thesis, Department of Geography*, University of Oslo, Norway.